Magnesium Technology 2011
Edited by: Wim H. Sillekens, Sean R. Agnew, Neale R. Neelameggham, and Suveen N. Mathaudhu
TMS (The Minerals, Metals & Materials Society), 2011

Magnesium Technology 2011

Corrosion and Coatings

Session Chairs:

Robert C. McCune
(Robert C. McCune and Associates LLC, USA)
Neale R. Neelameggham
(US Magnesium LLC, USA)

Magnesium Technology 2011
Edited by: Wim H. Sillekens, Sean R. Agnew, Neale R. Neelameggham, and Suveen N. Mathaudhu
TMS (The Minerals, Metals & Materials Society), 2011

SALT SPRAY CORROSION OF MECHANICAL JUNCTIONS OF MAGNESIUM CASTINGS

Sabrina Grassini, Paolo Matteis, Giorgio Scavino, Marco Rossetto, Donato Firrao
Politecnico di Torino – DISMIC department; 24 Corso Duca degli Abruzzi; Torino, It-10129, Italy

Keywords: AE44, galvanic corrosion, mechanical couplings

Abstract

The corrosion of cast, 3 mm thick, AE44 magnesium-alloy plates fastened to aluminum-alloy threaded counterparts, either constituting the screw or the nut, were tested in neutral salt spray for 48 hours, with or without interposed AA5051 spacers (washers). Steel nuts or screws were used, always insulating from corrosion the steel sides. Couplings between magnesium alloy plates and coated steel counterparts (screw heads) with interposed AA5051 washers were also tested, while insulating the nut side. Every 4 or 8 hours the test was halted and the samples were rinsed and photographed for manual image analysis. Then the plates were unmounted, slightly polished (highlighting the deep corrosion pits), and scanned for automatic image analysis. Different image analysis methods were compared. The least corrosion occurs, in couplings with aluminum alloy counterparts, when AA5051 washers are interposed; whereas the most effective coupling with steel counterparts is the one with nylon coated steel heads.

Introduction

A serious limitation to the application of magnesium alloys for the production of parts exposed to the environment is their susceptibility to corrosion, in particular when the alloy contains critical impurities, is coupled with other metals and is exposed to aggressive environments [1].

The corrosion of Mg and Mg alloys generally initiates as localized corrosion, while only in rare cases it is uniform and widespread. The poor corrosion behavior of Mg alloys derives from the following two main reasons.

Firstly, Mg and Mg alloys are generally susceptible to galvanic corrosion, which can be both internal and external. Low hydrogen overvoltage elements, such as Ni, Fe and Cu, that can be present as second phase and impurities in the alloy, or can be coupled with it, constitute efficient cathodes in contact with the magnesium anode, causing serious attacks. Instead, metals with high hydrogen overvoltage, like Al, Zn and Sn, can be less damaging [2]. The galvanic corrosion rate is increased by the conductivity of the medium, by a large potential difference and a small distance between the cathode and the anode, as well as by a large area ratio of cathode and anode [3].

Secondly, even if the quasi-passive hydroxide film can give a good protection in indoor and outdoor atmospheres, Mg alloys are characterized by a poor pitting resistance. Pitting corrosion occurs in the presence of chloride ions, both in neutral or alkaline salt solutions, e.g. seawater. The pitting corrosion resistance is influenced by the alloy's chemical composition and microstructure. In the case of Mg-Al alloys, such as AZ91 (which contains 9-10% of aluminum), pits are formed due to selective attacks along the primary intermetallic β-phase ($Mg_{17}Al_{12}$); the β-phase can act either as a micro-galvanic cathode increasing the corrosion rate, if present as small intergranular precipitates, or as an anodic barrier inhibiting the corrosion reaction, when it is more continuous, distributed homogeneously on the grain boundaries and present with high volume fraction [4].

Several technologies have been developed for improving the corrosion resistance of magnesium and its alloys, including coatings, surface treatments, and alloying.

Chromate conversion coatings are relatively simple and commonly used in the automotive industry and can lead to good corrosion performance. However, since the Cr^{6+} ion is toxic and carcinogenic, treatments with chromate compounds are undesirable for industrial safety control and environment protection. Recently, low pressure plasma treatments and PECVD (Plasma Enhanced Chemical Vapor Deposition) of organosilicon thin films, thanks to their versatility and their low environmental impact, have been proposed for corrosion prevention [5].

At the same time, alloying with Rare Earth (RE) elements, such as Lanthanum (La), Cerium (Ce), Yttrium (Y) and Neodymium (Nd), is increasingly used to enhance both the corrosion resistance and the mechanical properties. The addition of Y can markedly improve the corrosion performance of Mg-Al alloys, by forming intermetallic phases, both on the grain boundaries and on the grain bulk, able to improve the stability of the film forming on the surface of the β-phase, thus reducing the corrosion attack [6].

Finally, in automotive applications, Mg alloy parts are commonly assembled with either bare aluminum alloy counterparts or coated steel counterparts, with different design solutions being employed to reduce the likelihood of severe galvanic corrosion, including the usage of aluminum alloy spacers to avoid the direct contact between the Mg alloy and a counterpart with an higher hydrogen overvoltage, as well as the usage of non-conductive (i.e., polymeric) coatings on the counterpart.

The corrosion behavior of the AE44 magnesium alloy, developed by the Hydro company, mechanically joined with common automotive assembly counterparts, is examined here.

The general corrosion of the AE44 alloy has been previously studied in both salt water [4,9] and salt spray [9], and the galvanic corrosion of the same alloy coupled with either steel or aluminum alloys has been previously studied with polarization measurements [7] and free corrosion tests [8] in salt water. Therefore, this work aims to assess the effectiveness of different assembling methods, which could be applied in the automotive industry to limit the galvanic corrosion of this alloy in coupling with either aluminum alloy or coated steel counterparts, by subjecting several such assemblies to a salt spray environment.

Experimental Details

Samples Preparation

The examined AE44 Mg alloy [4] has the following nominal weight composition: 4% Al and 4% RE, with the following RE mixture: Ce > 50%, La 20 – 35%, Nd 10 – 20%, Pr 4 – 10%.

The Mg alloy was cast in the shape of 3 mm thick, 100 mm wide and 140 mm long plates, with 8.5 mm diam. trough holes, and was tested in the as-cast state, without any coating and without previous surface polishing.

Screws, or other male threaded parts, were mounted through the plates holes and fastened with nuts, or other female threaded parts, with or without washers (acting as spacers). All assembled items, except the plates themselves, were industrial components, or parts thereof. Either the screw side or the nut side of each assembly was exposed to the salt spray, and is described below; while the other side (made with aluminum washers and coated steel nuts or screws) was effectively sealed with a neutral silicone sealant (ISO 11600 standard).

Uncoated aluminum alloy spacers and uncoated aluminum alloy counterparts or coated steel counterparts were mounted as described in Table I and sketched in Figure 3 below (1st row).

Table I. Tested assembly types (or subtypes): tests number; metric thread and mounting torque; spacers and counterparts mounted on the Mg-alloy plates: material (steel and coating type, or aluminum alloy), thickness (Th.), inner and outer diameter (ID and OD).

type	tests	thread	torque	spacer (washer)				counterpart		
				alloy	Th.	ID	OD	alloy	coating	OD
-	#	mm	Nm	-	mm	mm	mm	-	-	mm
A	6	8	24	-	-	-	-	328.0	-	*
B	4	6	10	5051	2	6.5	22.6	328.0	-	18.6
C_1	2	18	24	†	1.6	18.5	23.4	2011	-	23.3
C_2	1	18	24	5051	2	18.5	23.4	2011	-	23.3
D_1	6	8	24	5051	2	8.5	25.5	steel	Zn-Al-Si 720 h‡	17.0
D_2	6	8	24	5051	2	8.5	25.5	steel	Zn-Al-Si 480 h‡	17.0
E	6	8	24	5051	2	8.5	24.2	steel	Zn, Nylon	16.2
F	6	8	24	5051	1	8.2	14.0§	steel	Zn	13.0

*Not circular †Unknown ‡Salt spray endurance §Contact area

The cast AA 328.0 counterparts (assembly types A and B) were cut from one automotive gear box with female threads; the wrought AA 2011 counterparts (type C) were oil plugs with a male thread (only in this case, the plate holes were enlarged to 18.5 mm diameter); and the steel counterparts were screw heads with different Zn-based coatings: either a plain Zn layer (type F), or a Zn inner layer and a polymeric outer layer (type E), or a Zn-Al-Si layer with 480 or 720 h nominal salt spray endurance (subtypes D_1 and D_2, respectively). Most spacers were plain washers, with the dimensions given in Table I; only the F assembly spacers were cup washers, 1 mm thick, with 8.2 mm hole diameter, 14 mm contact (plane) area outer diameter, 18 mm maximum outer diameter and 8 mm total axial height, with a large fillet radius between the contact area outer diameter and the maximum diameter. Most counterparts exhibited circular contact areas, with the diameters given in Table I, thus the path going from the counterpart edge to the Mg alloy plate, passing on the spacer, was constant along the same edge; only the A assemblies, which had no spacers, exhibited non-circular contact areas.

Salt Spray Tests

The 37 assemblies were mounted on 19 Mg-alloy plates, which were tested simultaneously on two polymeric racks placed in symmetric positions inside a 0.5 m^3 salt spray chamber, in accordance with the ASTM B117 standard. The plates were inclined of 30° in respect to the vertical. The two available mounting holes in each plate were vertically aligned in the rack, hence each assembly was either in a top (upstream) or bottom (downstream) position.

The 5 wt.% aqueous NaCl solution was prepared with deionized water and 97.7% pure NaCl (without Ni and Cu and with less than 0.1 wt.% NaI). The nozzle exit temperature was 48 °C and the chamber temperature was 35 ± 1.5 °C.

The test was halted after 4, 8, 16, 24, 32, 40 and 48 h of total salt spray exposure. After each stop, the chamber was rinsed with external air for 30 min to remove the salt spray, then it was opened and the samples were removed, rinsed with distilled water, dried with a compressed air jet, and photographed. Each plate was always tested in the same rack position. Since the samples were not subjected to a corrosive environment during the test stops, the overall salt spray test is deemed equivalent to a continuous test of equal total salt spray exposure time.

Image Analysis

All assemblies were photographed before the test start and after each test stop (after rinsing and drying), always with the same lighting, digital camera, camera settings, and angle of view. The assemblies were photographed from the direction perpendicular to the plate, except the A and B type assemblies, which exhibited large counterparts hiding the contact areas edges in such view, and were thus photographed from two mutually perpendicular directions forming angles of about 45° with the plate. 2288 x 1712 pixel, 24-bit RGB color, jpg compressed pictures, were recorded. The resolution of the perpendicular view pictures on the Mg-alloy plate plane was from 30 to 40 pixel/mm.

Then, the following quantitative analyses were performed on one assembly, mounted in a bottom position, for each type.

The pictures taken during the test stops were subjected to manual image analysis, by measuring the maximum linear dimension of each detectable corrosion pit in the plate region surrounding the contact area; a grand total of 1002 pits were measured.

Moreover, after the last salt spray test, the assemblies were unmounted and their Mg-alloy plates were first photographed in the same above-described manner (perpendicular view) and then polished with emery papers on a metallographic polishing machine (the plates were cut to reduce the area to be polished), in two successive steps, with 28 and 14 μm abrasive size, in order to remove both the salts and corrosion products and a surface layer about 50-100 μm thick. This included the layer affected by the original surface roughness and by most general corrosion effects,

but not the bottom of the corrosion pits due to localized corrosion close to the mechanical junction (as well as of some pits due to general corrosion), which were deeper. Hence, the latter corrosion pits were clearly evidenced as opaque areas against the reflective metallic background.

Thereafter, the polished plates were scanned on a flatbed image scanner, and 8-bit grey, jpg compressed pictures were recorded with a resolution of 24 pixel/mm and processed with an automatic image analysis software (ImageJ, http://rsbweb.nih.gov/ij) to identify the corrosion pits occurring inside the 10 mm wide annulus surrounding the contact circle, the annulus inner diameter being equal to the washer contact area OD (given in Table I). In the A-assembly case, a 10 mm wide band surrounding the irregularly shaped contact area was similarly examined.

The corrosion pits area fraction was calculated both for the whole examined annulus or band and as a function of the distance from the contact area boundary; for the latter purpose, the 10 mm annulus or band was divided into 20 adjacent 0.5 mm wide narrower annuli or bands.

Results and Discussion

Manual Image Analysis

Nominally equal assemblies at equal test times exhibited similar corrosion effects, as evaluated qualitatively during the tests and on the ensuing photographic documentation.

The results of the quantitative manual image analysis performed on one assembly for each type are shown in Figure 1. Within 4 to 8 h from the start of the test, the Mg-alloy plate exhibits general corrosion effects and develops a surface layer of corrosion products and/or deposited salt, while some corrosion pits are detected close to the contact area edge and grow in time; only in the A assembly a continuous corrosion groove already occurs on the contact area edge after 4 h test duration. Thereafter, both the largest and the mean pit size measured after each test stop either decrease or exhibit large oscillations, because the corrosion pits are at times partially or totally hidden by the salts and/or corrosion products deposited on the surface during the test (and not removed by rinsing). For this reason, after 16 h test duration, the actual corrosion pit development can hardly be inferred from the external appearance of the samples.

For example, the corrosion groove found on the whole contact area edge in the examined A type assembly after 4 h (Figure 2a) was then partially hidden and detected as a set of separate smaller pits after 24 h (Figure 2b); even if the former corrosion pit was evident again after the slight surface polishing performed at the end of the 48 h salt spray test (Figure 3 below).

Neglecting this problem, on the basis of the manual image analysis, and particularly of the largest and mean pit size measurements, the corrosion behavior was worst in the A and D assemblies and best in the E and F ones. Finally, at the end of the test, the unmounted A assembly exhibited corrosion effects on the plate area which was covered by the counterpart during the test, as shown in Figure 3, which were not accounted in the image analysis (both manual and automatic). Similar effects were much less evident, but not completely absent, in other assemblies.

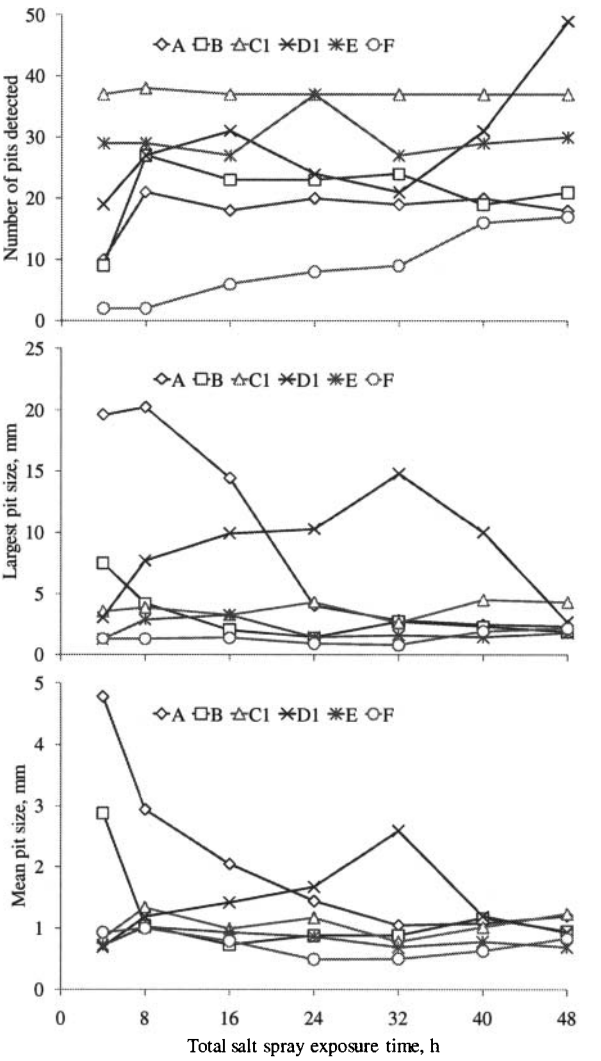

Figure 1. Manual image analysis. Number, largest size, and mean size, of the corrosion pits detected around the contact area after each test stop, for one assembly of each type (A to F).

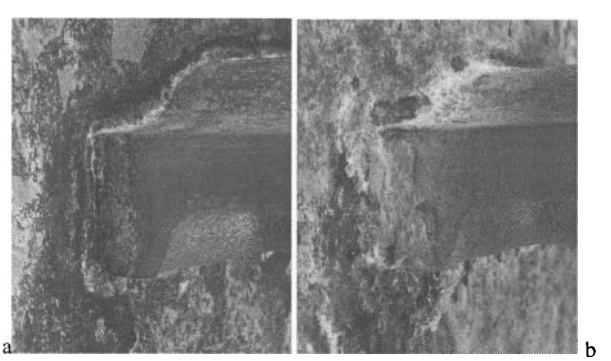

a b

Figure 2. Continuous corrosion pit along the contact area in a type A assembly after 4 h salt spray exposure (a); same region partially covered by salts and/or corrosion products after 24 h (b).

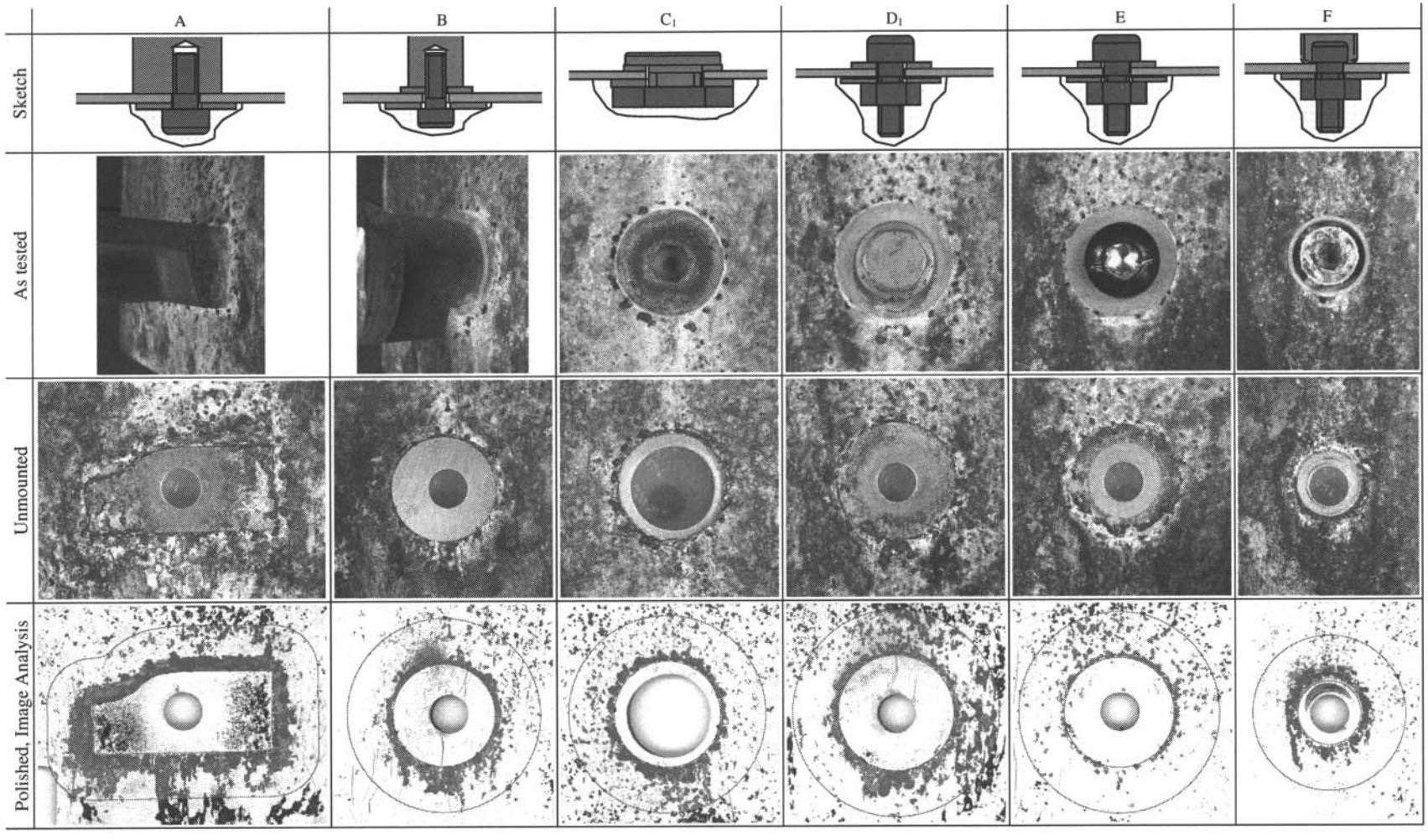

Figure 3. Photographic documentation and image analysis of 1 specimen for each assembly type (columns). Assembly sketches (row 1; Mg-alloy, Al-alloys, coated-steel and silicon and are shown in grey, blue, red and yellow, respectively). Digital-camera color pictures after 48 h salt bath exposure, rinsing and air drying (row 2) and after unmounting the counterpart and the spacer from the Mg-alloy plate (row 3); flatbed-scanner gray pictures after slight polishing of the Mg-alloy plate, highlighting the deep corrosion pits on the metallic background (row 4); and binary red/transparent pictures of the corrosion pits recognized by image analysis in a 10 mm wide region around the contact area (region bounded by red lines), superimposed on their corresponding gray pictures (row 4). Top-bottom pictures orientation as during the salt spray test. Pictures direction of view normal to the Mg-alloy plate and picture height on the plate plane 48 mm (magnification 0.77x) in all cases, except the A and B-type assemblies as-tested pictures (row 2, column 1 and 2).

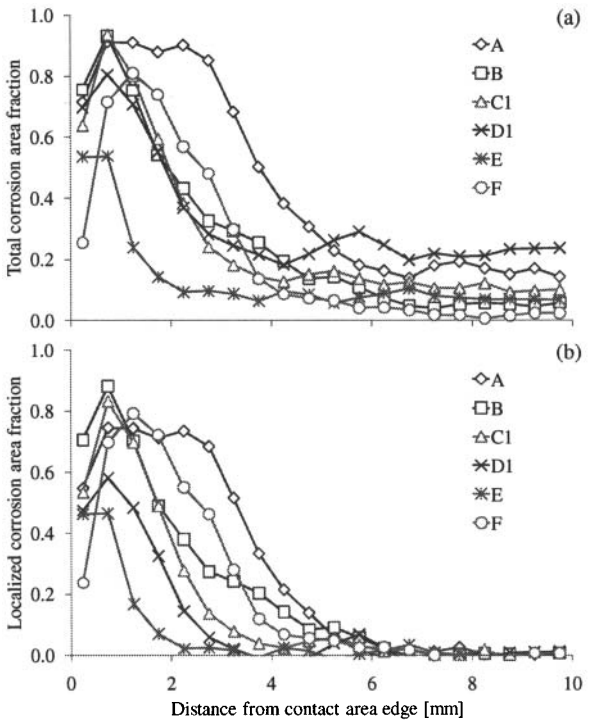

Figure 4. Automatic image analysis after 48 h salt spray exposure. Total corrosion area fraction (AF), at increasing distance from the mechanical junction (a), and AF due to localized corrosion only (b); 1 specimen for each assembly type (A to F).

Automatic Image Analysis

The results of the automatic image analysis, performed after the 48 h salt spray test, are given in Figures 3 and 4 and Table II.

In Figure 3, the polished plate surfaces are compared with the same regions photographed before polishing, both at the end of the test and after unmounting the counterparts and spacers, and with the corrosion pits recognized by image analysis in the 10 mm wide region around the contact area, showing that the polishing and automatic image analysis procedures were generally effective for the purpose of evidencing the deep corrosion pits. On the basis of the overall corrosion pits area fraction in the examined region, which ranges from 12 to 40 % (Table II), the six assembly types can be rated in the following order of apparent increasing corrosion sensitivity: E, F, B, C_1, D_1 and A. However, the latter results do not always discriminate the localized corrosion features related to the mechanical junction from the surrounding general corrosion ones.

This problem is addressed in Figure 4, where the corrosion pits area fraction is plotted as a function of the distance from the mechanical junction. The corrosion area fraction always exhibits an initial maximum due to localized corrosion, and then decreases to a lower value, due to general corrosion, which becomes almost constant (for each sample) at distances larger than 6 mm. Most often the maximum corrosion area fraction (Figure 4a and Table II) is detected in the 2nd nearer annulus or band, rather than in the 1st one, in respect to the junction edge; this is likely an artifact due to small deviations between the inner boundary of the 1st annulus or band and the actual contact area boundary, in turn due to geometrical irregularities of the latter boundary (this phenomenon is the most evident in the F assembly, in which the contact area boundary is the least clearly defined due to the lack of a sharp edge in the cup washer).

The general corrosion area fraction, defined as the mean corrosion area fraction in the 7 to 10 mm distance range from the junction, ranges from 2 to 22 % in different plates (Table II), likely due to the different sample positions in the salt spray chamber and/or to a more or less complete removal of the shallower general corrosion features during the polishing procedure. Thus, in Figure 4b the same data (already shown in Figure 4a) are plotted again after subtracting the general corrosion area fraction of each sample, in order to show only the contribution (to the total corrosion) due to the localized corrosion at the junction edge.

The latter plot, Figure 4b, evidences that the A, B, C_1 and F type assemblies all cause localized corrosion effect on more than 74% of the Mg-alloy surface near the junction edge, whereas the same measure is 58 and 47% in the D_1 and F assemblies, respectively (Table II). Moreover, the width of the region affected by localized corrosion, defined as the distance from the junction at which the localized corrosion area fraction eventually falls below half of its maximum value, is the largest in the A and F assemblies and the smallest in the E assembly (Table II).

Table II. Automatic image analysis after 48 h salt spray exposure. Mean and maximum total corrosion Area Fraction (AF) within 10 mm from the mechanical junction, AF due to general or localized corrosion only, and width of localized corrosion region; 1 specimen for each assembly type (A to F).

Corrosion type	Measure	Assembly type					
		A	B	C_1	D_1	E	F
Total	mean AF, %	40	22	23	31	12	17
	max. AF, %	91	93	94	81	54	81
General	mean AF, %	17	5	10	22	7	2
Localized	max. AF, %	74	88	83	58	47	79
	width, mm	3,5	2	2	2	1	3

Thus, by subtracting the contribution of the general corrosion, and by considering both the localized corrosion maximum area fraction and width of affected area (Figure 4b and Table II), the six assembly types can be rated in the following order of increasing corrosion sensitivity: E, D_1, C_1, B, F and A.

This latter order is different, and is deemed more correct, that the order which could be obtained both from the overall corrosion pits area fraction measured in the examined region after the salt spray test, and from the manual image analysis of the junctions photographed during the test stops, because the latter methods do not discriminate the localized effects, which are due to the mechanical junction, from the general effects, which may be different due to experimental details.

This correction is especially important in the examined F assembly type specimen. In fact, this was rated among the least affected by corrosion both on the basis of the manual image analysis of the assembled junctions and on the basis of the overall corrosion area fraction in the region examined by automatic image analysis. However, from Figures 3 and 4 it can be noted that the

former observation was misleading because the localized corrosion occurring under the curved surface of the cup washer was almost completely hidden by the top edge of the same washer (Figure 3), whereas the latter measure was misleading because the specimen exhibited the least general corrosion contribution and the smallest contact area OD (hence the area closer to the junction was the smallest fraction of the total examined area).

Conclusions

Test Methods Effectiveness

The manual image analysis of the specimens exposed to the salt spray test for increasing durations was not reliable, because the actual extension of the localized corrosion effects was soon hindered by a layer of corrosion products and/or deposited salt, not removed by rinsing in water, and was hidden by the assembly itself in the case of the cup washer.

A slight polishing of the (unmounted) Mg-alloy plate, performed after the salt spray test, was effective to highlight the deep opaque corrosion pits against a reflective metallic background, allowing to perform quantitative automatic image analyses. Moreover, a plot of the corrosion pits area fraction against the distance from the edge of the contact area (between the Mg-alloy plate and the counterpart or spacer), up to 10 mm distance, obtained from the latter image analysis, allowed to effectively measure and compare the localized corrosion at the edge of the mechanical junction, notwithstanding differences among different specimens in the amount of general corrosion effects detected further away from the junction, likely due to differences in the salt spray test severity (due to different positions in the test chamber) and/or in the polishing procedure. On the contrary, the overall corrosion pits area fraction of the same 10 mm wide examined region is less significant, because the surrounding general corrosion introduces a variable and possibly large contribution to this measure.

Localized Corrosion Mechanisms

Localized corrosion close to the boundary of the contact area (between the Mg-alloy plate and the counterpart or spacer) was detected in all tested assemblies.

In most cases, the contact area boundary was defined by a sharp edge of the counterpart or spacer, and the corrosion occurred immediately outside, but not immediately inside, such edge, on the plate surface which was directly exposed to the salt spray, hence it is attributed to galvanic corrosion.

However, in the F assembly, in which a cup washer was used as a spacer (between the Mg-alloy plate and a coated steel counterpart), the corrosion occurred mainly in the interstice between the cup itself and the plate, and is attributed to a combination of galvanic corrosion and crevice corrosion.

Furthermore, some crevice corrosion was also detected, although not measured, in the A assembly, in which there was no spacer, on some Mg-alloy plate areas, which were not adjacent to the contact area edge and were completely covered by the cast aluminum alloy counterpart.

Spacers Effectiveness

The comparison of the B and A type assemblies, in which the same 328.0 cast aluminum alloy counterpart was mounted with or without interposed 5051 (AlMg2) wrought aluminum alloy spacers, respectively, allows to conclude that the latter spacers were effective to reduce the localized corrosion, both by reducing (from 3.5 to 2 mm) the width of the deeply corroded region adjacent to the junction, and by avoiding the occurrence of crevice corrosion (which was found only in the A assembly contact area, as mentioned above).

This conclusion is further corroborated by the fact that the localized corrosion observed in the other assemblies, which all mounted aluminum alloy spacers, albeit with different counterparts, was always less than that observed in the A assembly type.

Moreover, the comparison between the F assembly, exhibiting a cup-washer spacer, on one side, and the D and E assemblies, exhibiting plain-washer spacers, on the other side, all with coated steel counterparts (albeit with different coating) allows to conclude that the plain washer geometry is much more effective than the tested cup washer one, because the latter favors the crevice corrosion.

However, the crevice corrosion arises here because the employed cup washer exhibit a large fillet radius at the contact area edge, thus creating an interstice with the Mg-alloy plate; hence it is not excluded that cup washers with a sharp contact area edge may be more effective than plain washers, by imposing a longer path between a low hydrogen voltage counterpart and the magnesium alloy.

Assemblies with Aluminum Alloy Counterparts

Among the 3 tested assemblies with aluminum alloy counterparts, the A assembly, with a 328.0 cast aluminum alloy counterpart and without any spacer, clearly exhibits the worst corrosion behavior; whereas the corrosion behaviors of the B and C assemblies, with 5051 (AlMg2) aluminum alloy spacers and cast or wrought aluminum alloy counterparts, is almost equal; hence, the usage of such spacers is recommended.

Assemblies with Coated Steel Counterparts

Among the 3 tested assemblies with coated steel counterparts, all with bare aluminum alloy spacers, the E assembly, with a zinc and nylon double coating applied on the steel counterpart, clearly showed the best corrosion resistance, whereas the F assembly, with the cup-washer spacer, was the worst due to the above described crevice corrosion issue, and the D assembly with the Zn-Al-Si coating was intermediate. In particular, the corrosion behavior of the E assembly was the best of all examined assemblies (with both aluminum alloy and coated steel counterparts).

Acknowledgements

A. Regis and I. Orsingher, Magnesium Products of Italy (MPI) S.p.A, Verres, Aosta, Italy, for material procurement and useful discussion.

References

1. G.L. Song and A. Atrens, "Corrosion Mechanism of Magnesium Alloys", Advanced Engineering Materials, 1 (1999), 11-33.
2. A. Froats, T.K. Aune, D. Hawke, W. Usworth and J. Hillis, in Metals Handbook, 9th ed., Vol.13, ASM Int., Material Park, OH, USA, 1987, 740-754.
3. W.S. Loose, in: Corrosion and Protection of Magnesium, ASM Int., Materials Park, OH, USA, 1946, 173-260.
4. R.B. Alvarez, H.J. Martin, M.F. Horstemeyer, M.Q. Chandler and N. Williams, "Corrosion relationship as a function of time and surface roughness on a structural AE44 magnesium alloy", Corrosion Science, 52 (2010), 1635-1648.
5. E. Angelini, S. Grassini, F. Rosalbino, F. Fracassi and R. D'Agostino, "Electrochemical impedance spectroscopy evaluation of the corrosion behaviour of Mg alloy coated with PECVD organosilicon thin film", Progress in Organic Coatings, 46 (2003), 107-111.
6. T.J. Luo, Y.S. Yang, Y.J. Li and X.G. Dong, "Influence of rare earth Y on the corrosion behavior of as-cast AZ91 alloy", Electrochimica Acta, 54 (2009), 6433-6437.
7. K.B. Deshpande, "Validated numerical modelling of galvanic corrosion for couples: Magnesium alloy (AE44)–mild steel and AE44–aluminium alloy (AA6063) in brine solution", Corrosion Science, 52 (2010), 3514–3522.
8. K.B. Deshpande, "Experimental investigation of galvanic corrosion: comparison between SVET and immersion techniques", Corrosion Science, 52 (2010), 2819-2826.
9. H.J. Martin, M.F. Horstemeyer and P.T. Wang, "Comparison of corrosion pitting under immersion and salt-spray environments on an as-cast AE44 magnesium alloy", Corrosion Science, 52 (2010), 3624–3638.